energies

MDPI

Article

Investigating the Parameter-Driven Cathode Gas Diffusion of PEMFCs with a Piecewise Linearization Model

Siwen Gu [1,2], Jiaan Wang [1], Xinmin You [3] and Yu Zhuang [2,*]

[1] School of Photoelectric Engineering, Changzhou Institute of Technology, Changzhou 213032, China
[2] Frontiers Science Center for Smart Materials Oriented Chemical Engineering, Institute of Chemical Process Systems Engineering, School of Chemical Engineering, Dalian University of Technology, Dalian 116024, China
[3] Fundamental Aspects of Materials and Energy (FAME), Faculty of Applied Sciences, Delft University of Technology, Mekelweg 15, 2629 JB Delft, The Netherlands
* Correspondence: zhuangyu@dlut.edu.cn

Abstract: Improving mass transfer in gas diffusion layers is critical to achieving high-performance proton-exchange membrane fuel cells (PEMFCs). Leaks through the interface between the gas and the membrane electrode assembly frame have been widely investigated, and the controllability of the cathode gas diffusion has not been achieved in most studies. In this study, we develop a structural parameter to investigate the controllability of the gas diffusion mechanism in the cathode in order to improve upon the design and performance of PEMFCs. This parameter accounts for the cathode gas diffusion layer porosity and carbon loading inside the catalyst layer. It is comprehensively calculated to relax the two segments' distribution along three directions of the coordinate axis. The experimental and simulation results show that the obtained values of the parameter vary and change during voltage stabilization. According to the results, regardless of the materials in the cathode gas diffusion layer, the same steady-state voltage is obtained when the parameter is fixed. The cell could be controllably operated for a wide range of diffusion layer thicknesses by selecting the optimal parameter.

Keywords: PEMFC; structural parameter; gas diffusion; cathode; simulation

Citation: Gu, S.; Wang, J.; You, X.; Zhuang, Y. Investigating the Parameter-Driven Cathode Gas Diffusion of PEMFCs with a Piecewise Linearization Model. *Energies* **2023**, *16*, 3770. https://doi.org/10.3390/en16093770

Academic Editor: Antonino S. Aricò

Received: 7 March 2023
Revised: 24 April 2023
Accepted: 27 April 2023
Published: 28 April 2023

1. Introduction

Despite the advances in science, technology and economics in recent decades, environmental and energy problems have become more prevalent. In order to avoid the consequences of these crises, we must become environmentally responsible as soon as possible. In order to achieve this, we need to develop sources of alternative green energy and redirect ourselves off the path of reckless fossil fuel consumption. Currently, there are many promising forms of new energy technology being looked at as possible replacements for fossil fuels, one of which is the proton-exchange membrane fuel cell (PEMFC) [1,2]. The PEMFC is a type of power-generating device that converts the chemical energy of a fuel and oxidant directly into electrical energy by the process of electrochemical reaction while benefiting from a high energy density, a low operating temperature, and a long operational lifespan [3]. However, though the principles behind the PEMFC are quite simple, it remains unknown how the performance of PEMFC is influenced by many variables that factor into its ability to operate effectively. This necessitates the development of a model to determine the gas diffusion mechanisms so that the controllable operation of PEMFCs is ensured.

To date, most of the research on PEMFC models has focused on the gas diffusion layer. Jiao et al. [4] proposed a gas–liquid–solid coupled solver to describe the liquid water transport, vapor condensation, conjugate heat transfer, electric conduction, and their interactions. Deng et al. [5] developed data-driven surrogate models that were established on the basis of the simulation results of a three-dimensional validated numerical model. Additionally, the gas distribution quality was evaluated by the values of mean and standard deviation of the reactant gas concentration in the catalyst layer. From the view of

a high-temperature polymer electrolyte membrane fuel cell (HTPEMFC), Herdem et al. [6] developed a methanol reformer system and investigated the influences of the reformate gas composition on the performance of HTPEMFC at different temperatures.

It is well known that the compressed gas diffusion lays are strongly influenced by the water transport problem from the point of view of drainability. Thus, a large body of work has focused on developing models to describe the water transport inside gas diffusion layers. Xu et al. [7] developed an integrated model to predict the water transport in a nonuniform compressed gas diffusion layer. For simulating fuel cell performance, Rahman et al. [8] established a steady-state and two-phase model that was employed to simulate the interaction between gas and liquid transports. From the view of background on the characteristics of the gas diffusion layer, Cindrella et al. [9] considered the influence of these characteristics on water management in the PEMFC. Xu et al. [10] investigated the effects of a wave-shaped flow channel structure and a groove in the gas diffusion layer.

Based on these studies concerning models of the gas diffusion layer, it is clear that the model parameters also have an obvious effect on the performance of PEMFCs. Thus, proper distribution of parameters can be beneficial to improve such performance. For the cathode gas diffusion layer, He et al. [11] developed a 3D model to investigate the parameters affecting the cell performance. The results showed that an increasing ratio of platinum to carbon resulted in a decrease in the activation and concentration overvoltage, and had little influence on the ohmic overvoltage. For surface modifications, Wang et al. [12] considered a dimeric ionic liquid di-nonafluorobutanesulfonate on a PtCo/C catalyst so as to improve the performance and durability of the catalyst in a fuel cell membrane electrode assembly (MEA). Additionally, the electrochemically active surface area, impedance, and gas diffusion resistance were analyzed. Moreover, the PEMFC contamination effect is helpful to promote the economy and utilization efficiency. Matamoros and Brüggemann [13] investigated the concentration and ohmic losses in free-breathing PEMFC under different operating conditions. Zhou et al. [14] suggested that the voltage loss distributions were crucial to improving the PEMFC performance. Additionally, they studied the influences of the local operating state on the distributions of output voltage and voltage losses. Based on their works, Pan et al. [15] proposed a flow field analysis scheme including two dimensionless configuration parameters that were employed to ensure the flow distribution. Considering the influence of performance degradation, Sun et al. [16] developed a three-dimensional, multi-component, and multi-physics PEMFC model. With this model, different degradation conditions, such as flooding, dehydration, and PEMFC aging, were simulated, respectively. Similarly, Ma et al. [17] proposed a hybrid prognostic approach to predict the output voltage and other aging parameters affecting the internal degradation.

Based on the above literature, the studies on the model for gas diffusion have focused on the promising accuracy and simulation results of a numerical model. The optimization calculation of a new parameter to be guided by the controllable operation in PEMFCs has not been found in previous papers. To address this scientific question and the issues mentioned above, this work aims to provide a comprehensive understanding of the effects of a new structural parameter on PEMFC operation. First, in Section 2, the combinatorial complexities associated with the different overvoltages are disentangled from the formulation through a gas diffusion simulation. Additionally, the major influencing factor for the change in voltage over time is determined through the structures and mechanisms within the PEMFC using mathematical models. A piecewise linearization model, including the new structural parameter, is established in the next section. The experimental and dynamic simulation results shown that this parameter is related to the oxygen permeation capacity through the PEMFC, which is, in turn, influenced by the properties of the electrode material, shown in Section 4.

2. Simulation of the Membrane Electrode Assembly

The simplified models in this section are based on an MEA, which includes the following three domains: a cathode, a separator, and an anode, as shown in Figure 1. The

separator comprises of two gas diffusion layers, two catalyst layers and one PEM [18]. The red arrow along the MEA indicates the inlet to outlet direction of the cathode gas. Gas diffusion is presented between the catalyst and current collector on the cathode and anode sides. Oxygen reduction reactions and hydrogen oxidation reactions occur inside two different areas of the catalyst, respectively [19].

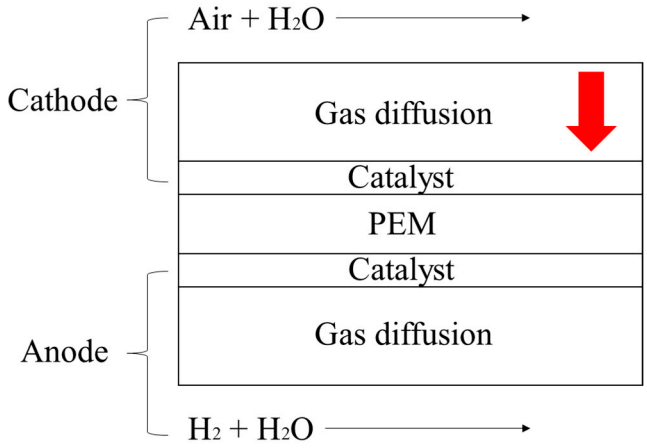

Figure 1. Schematic model of the numerical simulation.

Cathode: $\frac{1}{2}O_2 + 2H^+ + 2e^- \rightarrow H_2O$
Anode: $H_2 \rightarrow 2H^+ + 2e^-$

As a key tool in engineering and science innovation, simulations have an important effect on cost and time management, as they are far cheaper and faster than experimental analyses [20]. This section is detailed via a 3D model in COMSOL Multiphysics software. The main objective is to analyze the impact of cathode gas diffusion on the overvoltage. Therefore, only an analysis of the overvoltage and the molar concentration distribution of oxygen in cathode gas diffusion is presented. The PEMFC simulation code inside the software includes a continuity equation, the Brinkmann equation, the Maxwell-Stefan equation, and the Butler–Volmer equation [21]. The set of model descriptions and governing equations can be found in the work of Nishimura et al. [22]. In addition, in the following simulation, it is assumed that all oxygen atoms that diffuse through the gas diffusion layer immediately react and that electrons are saturated as soon as oxygen comes into contact with the catalyst layer.

Figure 2 shows the oxygen density over the PEMFC as mentioned above simulation code inside the software. The direction of cathode gas diffusion is placed the same as in Figure 1. From input to output, the molar concentration distribution of oxygen decreases due to the electrochemical energy generation reaction [23]. Additionally, the oxygen concentration decreases along with the gas flow. This concentration is located in the middle of the cathode with an overvoltage of 0.9 V. The minimum molar concentration distribution is given as the minimum in the same overvoltage. It is noted that when designing the features and setting the parameters of a PEMFC system, one must take both the transient and steady-state conditions within the fuel cell with regard to the cathode flow into account. However, the switching behavior among different concentrations consumes an unknown amount of time, so the controllable operation for PEMFCs has not yet been realized. It is crucial to define a new parameter so as to relax the relationship between the gas diffusion and the performance of the PEMFC.

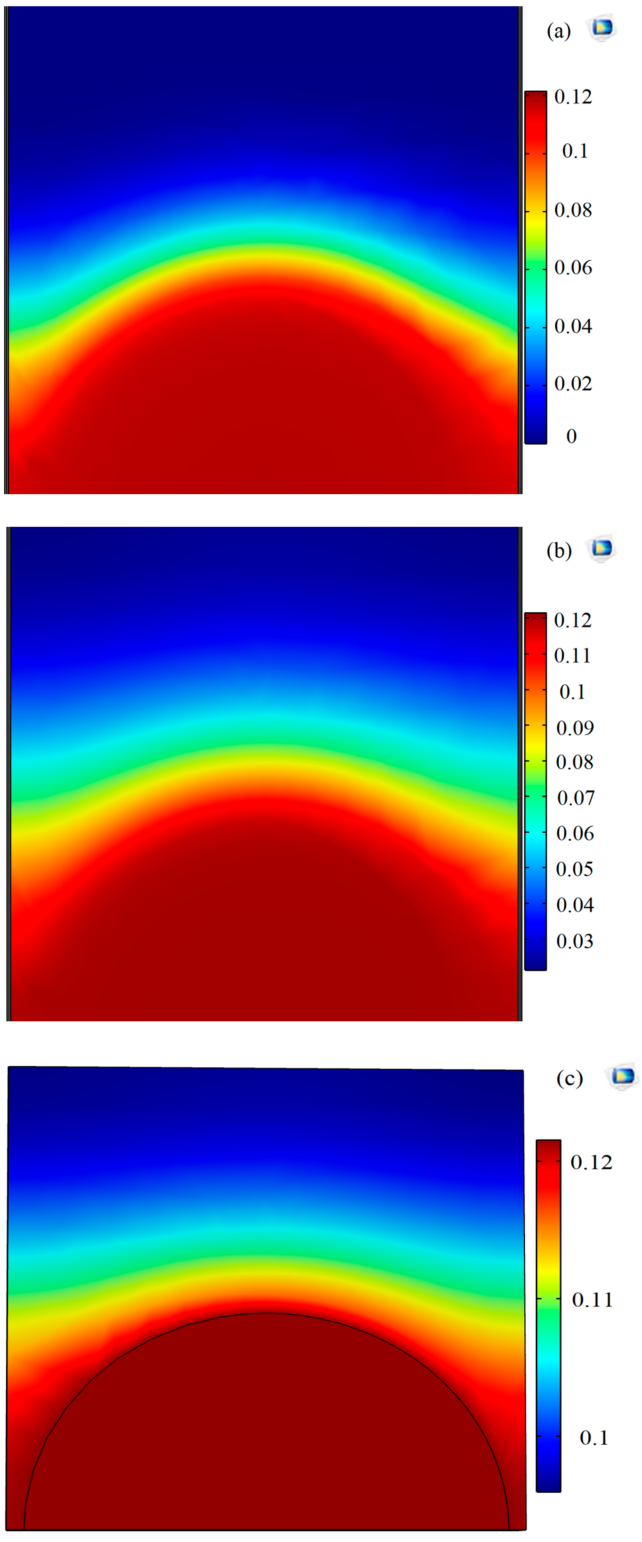

Figure 2. Top view of the oxygen concentration at (**a**) 0.5 V, (**b**) 0.7 V, and (**c**) 0.9 V.

3. Model Development

In order to characterize a structural parameter for the PEMFC, two sets of models are proposed for cathode gas flow and open circuit voltage, respectively. These models are established based on MEA with mass conservation and charge conservation, and are detailed in the following sections.

3.1. Cathode Flow Model

In a PEMFC, the number of electrons transferred between electrodes is equal to four times Avogadro's constant for each mole of oxygen that reacts. The flow rate of the number of reacted moles of oxygen, N, can be described by the following equation [24]:

$$\frac{dN}{dt} = \frac{I}{4\mathrm{N_A e}} \tag{1}$$

where I is the individual cell current (A), t is the time in seconds (s) that it takes for oxygen to flows over the electrode, $\mathrm{N_A}$ is Avogadro's constant (6.022×10^{23} mol^{-1}) [25], and e is electron charge (1.6×10^{-19} C) [26].

The actual amount of oxygen that reacts in an electrode depends on the area and layout of the flow path within the electrode. This means that the amount of supplied oxygen that an electrode actually uses varies significantly and is theoretically always less than one hundred percent of what is supplied. A coefficient that describes the relation between supplied oxygen and used oxygen is defined. In this work, such actual-oxygen-supply-coefficient is represented by α. The supplied oxygen volumetric flow rate can be expressed as follows:

$$\gamma = \frac{5.8 \times 10^{-5} I}{\alpha} \tag{2}$$

where I denotes the individual cell current in the unit of (mA) and γ is the oxygen volumetric flow rate (mL/s). α depends on the gas diffusion layer properties, the structure of bipolar plates, and the flow rate, so it is defined as follows:

$$\alpha = \theta \cdot \varphi \tag{3}$$

where θ is the permeation capacity of gas through a specific diffusion layer. The value depends on the material properties of the diffusion layer and its structure. φ denotes the flow influence factor, which is directly proportional to the gas pressure, the temperature, and the effective surface area of the diffusion layer.

The pressure of gas within a pipeline can be obtained using Bernoulli's equation as follows [27]:

$$P = \mathrm{C} - \rho\frac{\beta^2}{2} \tag{4}$$

where P represents the gas static pressure (Pa), C denotes the total pressure at an arbitrary point (Pa), which is a constant for a given system, β is the gas velocity (m/s), and ρ is the gas density (1.429 $\mathrm{kg/m^3}$) [28].

The flow influence factor φ can be derived from Equation (4) as follows:

$$\varphi = \mathrm{C}ST - \frac{10^{-12} S\rho T\gamma^2}{2D^2} \tag{5}$$

where T is the temperature of a single cell (K), S is the effective surface area of the electrode ($\mathrm{m^2}$), and D is the area of the gas tunnel cross-section ($\mathrm{m^2}$). Substituting Equation (5) into Equation (3) yields the following:

$$\alpha = \theta\mathrm{C}ST - \frac{10^{-12}\theta ST\rho\gamma^2}{2D^2} \tag{6}$$

Substituting Equation (6) into Equation (2), the relationship between the electrode current and the volumetric flow rate of supplied oxygen can be described as follows:

$$I = 17241\gamma\theta\mathrm{C}ST - \frac{8.62 \times 10^{-9}\theta ST\rho\gamma^3}{D^2} \tag{7}$$

3.2. Open Circuit Voltage Model

Generally, electrochemical models and physical chemistry models are used to describe the voltages of single-celled PEMFCs in a closed circuit as follows [29]:

$$V_{\text{cell}}(t) = E - V_{\text{act}} - V_{\text{ohmic}} \tag{8}$$

where V_{cell} is the fuel cell voltage (V), E is the electrode potential or thermodynamic potential (V), V_{act} is the activation overvoltage (V), and V_{ohmic} is the ohmic overvoltage (V).

An open circuit voltage model is introduced in this paper, as we mainly wish to study the influence of gas diffusion and the properties of the diffusion layer on the fuel cell voltage. The influence of water on the system is assumed to be negligible; that is, the activity of water is equal to one. Then, a simplified Nernst equation can be used to describe the thermodynamic potential. For an ideal gas, the reactant activity can be described by the ratio of the partial pressure of the gases to the standard pressure. By incorporating this into a simplified Nernst equation, the thermodynamic potential detailed by a piecewise linearization model as follows:

$$V_{\text{cell}}(t) = \begin{cases} 0, & t < t_0 \\ E^0 + \frac{RT}{2F} \ln(P_{H_2} P_{O_2}^{\frac{1}{2}}), & t > t_0 \end{cases} \tag{9}$$

where E^0 is the standard electrode potential (V). t denotes the reaction time (s), and t_0 represents the penetration time (s), or the time, in seconds, which oxygen atoms take to diffuse through the diffusion layer. R is the ideal gas constant (8.3 J/mol·K), F is the Faraday constant (96,485 C/mol). P_{H_2} is the hydrogen partial pressure (bar), and P_{O_2} is the oxygen partial pressure (bar). When using this equation, we assume that the ions can immediately transfer through the NAFION membrane and reach saturation as soon as oxygen arrives at the catalyst layer.

The penetration time t_0 is further described by the volumetric oxygen rate and the actual oxygen supply coefficient as follows:

$$t_0 = \frac{2 \times 10^6 dD^2}{2\gamma\theta CTD^2 - 10^{-12}\theta T\rho\gamma^3} \tag{10}$$

where d is the thickness of the diffusion layer (m).

The penetration time can be obtained in experiments, so the oxygen permeation capacity can be calculated by Equation (10).

4. Experiments and Discussions

In this section, on the one hand, two experiments that are designed to explore the impact of gas diffusion on the performance of the PEMFC are described. The time dependence of the MEA cell voltage was investigated, as well as the influence of the diffusion layer thickness on the penetration time, t_0. On the other hand, the verification of the suggested models is applied to the dynamic simulations. The proposed models containing the designed structural parameters to describe the penetration time and oxygen supply flow are implemented in a MATLAB/Simulink environment [30], and simulations are carried out for different periods of operation.

Two identical MEAs are constructed on a single membrane, and extra diffusion layers are then added to the MEAs but on opposite sides. Both MEAs are exposed to non-flowing hydrogen gas on one side. The MEA used in this experiment is composed of NAFION 115 membranes, a JM20% Pt/C catalyst, and TP-060 carbon paper [31]. The platinum loading is 1.5 mg/cm^2, and the effective area of the MEA is 9 cm^2. Different diffusion layer thicknesses are selected to represent the processes, i.e., 1.25 mm, 2.50 mm, and 3.75 mm.

The experiment proceeded as follows. First, both sides of the MEA were cleaned with nitrogen in order to ensure the system was clean. In the meantime, the MEA was kept in short-circuit to ensure that no free ions remained in the MEA; in other words, the initial

voltage was zero. Finally, the hydrogen valve is turned on and the flow rate is allowed to stabilize before oxygen is supplied, and the timer is started.

As shown in Figure 3, the voltage data of the three group MEAs with different total thicknesses of the diffusion layer is compared. In the first stage, $t < t_0$, the oxygen gradually permeates through this diffusion layer and has not yet reached the catalyst layer, so that the voltage at this time remains zero. The duration of this stage reflects the rate of oxygen penetration through the gas diffusion layer, as well as the actual-oxygen-supply-coefficient for the specific electrode material. In the second stage $t = t_0$, the oxygen has reached the catalyst layer, and a small molar concentration for the reaction is required by calculating the model. At this moment, it can be assumed that the electrons immediately have saturation after the oxygen reaches the catalyst layer, which is the voltage reaches the steady-state value. In the last stage, $t > t_0$, the voltage is maintained at the steady-state value. However, the electrode voltage is directly affected by decreasing the water content of the proton membrane in the reaction procedure, such as the water content of the proton membrane. Therefore, the steady-state voltage is less than the standard electrode potential in the actual operation.

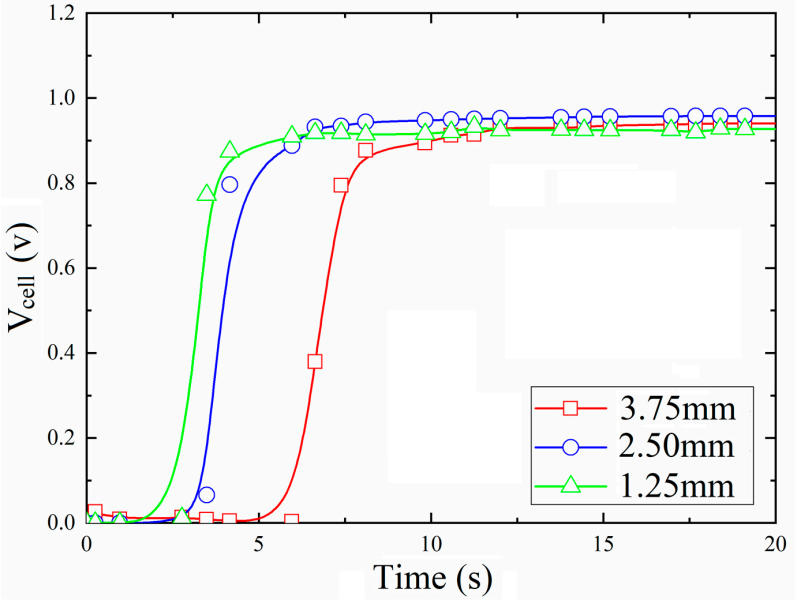

Figure 3. Voltage with different total thicknesses of the extra diffusion layer.

Then, the relationships between the properties of the carbon support and the voltage are compared by selecting different carbon surfaces. It is noted that this paper focuses on the distribution of reaction gas directly on the electrode surface rather than on new materials or new carbon surfaces. Therefore, external diffusion layers are constructed upon the electrode, with single-layer thicknesses of 0.14 mm, 0.25 mm, and 0.42 mm from different material manufacturers, respectively. Due to such different thicknesses, the consistent total thickness of the diffusion layer is given in these three groups by adjusting the number of carbon supports. The parameters of three carbon supports are given in Table 1 and a comparison is shown in Figure 4.

Table 1. Comparison of different carbon papers.

Carbon Support	Thickness (mm)	Electrical Resistivity (mΩ/cm^2)	Gas Permeability (mL·mm/cm^2·h·mmAq)
1	0.14	3.0	187
2	0.25	5.8	3250
3	0.42	3.6	1236

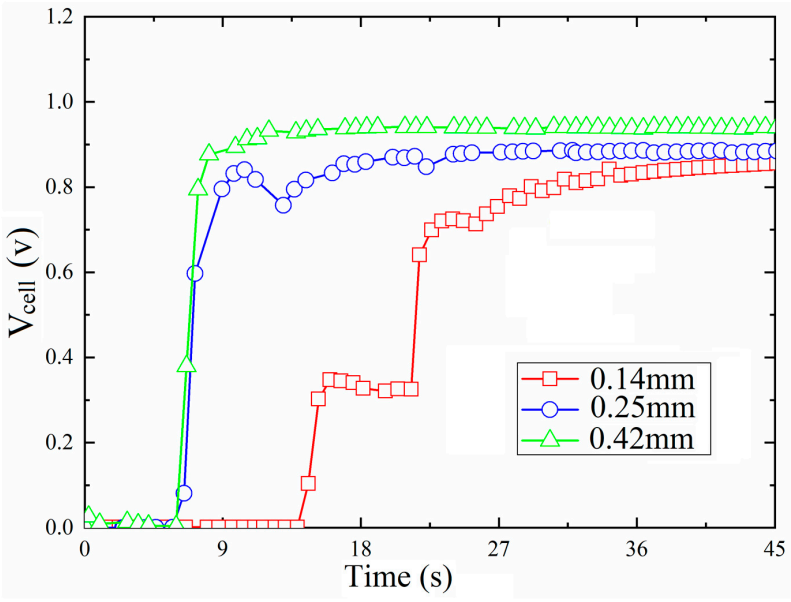

Figure 4. Voltage with the same total thickness of different types of carbon paper with different types.

As shown in Table 1, different electrical resistivity and gas permeability are found due to different thicknesses of carbon supports. The largest thickness is exhibited by the third one so that no additional layers of carbon supports in the corresponding electrode are needed to achieve the same total thickness as the other two electrodes. This makes the intermediate electrical resistivity and gas permeability comparable to the other two carbon supports. Similarly, in the second one, fewer layers of carbon supports represent fewer gaps among several layers due to incomplete fit. The other reason for such difference is the internal performance, which adopted the TGP-060 from Toray, a material manufacturer that provides cutting-edge materials. The above analysis can be also found in the comparison of the duration for the gas diffusion in Figure 4. Oxygen diffusion occurs in the second carbon surface immediately after it occurs in the first one. Then, the discontinuity in the oxygen diffusion is reduced, and the voltage is also relatively stable. The smallest thickness is given in the first carbon support, and more carbon supports are needed to form the electrode having the same total thickness as the others. As a result, the increased layers of carbon supports represent contain a large number of gaps due to an imperfect fit; thus, the duration is found to be longer, and the voltage is relatively unstable during the process of reaching a steady-state. Another reason for the unstable voltage could be related to the performance of this carbon support regarding the gas permeability, which negatively affects oxygen diffusion. Hence, the different duration for the gas diffusion, electrical resistivity, and gas permeability are demonstrated in the three carbon supports.

After comparing the voltages of the electrodes with different carbon supports, it is concluded that the steady-state value of the voltage is fixed along with the total thickness of the gas diffusion layer and the different performance of carbon supports. The materials and thickness of the gas diffusion layer each have the potential to influence the time to reach the catalyst layer and the duration of oxygen diffusion, as well as the process of obtaining a steady-state.

Furthermore, the verification of the suggested models is applied to the dynamic simulations. The feasibility of the open circuit voltage model based on the gas diffusion is investigated. The modeling and simulation of PEMFC operation are developed and performed in a Simulink environment and validated through the above experimental data. Due to the simplifying assumptions, the voltage of the fuel cell can be represented as the open circuit voltage. The model built in Simulink is obtained from the above equations and is shown in Figure 5. For both the cathode and anode of overvoltages, there are two subsystems in which the input parameters are required. Where the input consists

of hydrogen and the oxygen flow, the oxygen diffusion factor, the electrode temperature, current and electrode area. The output is the electrode voltage. In the cathode simulation model, the input includes the actual oxygen supply coefficient, the temperature, the oxygen flow rate, and the current, and the output is the oxygen partial pressure.

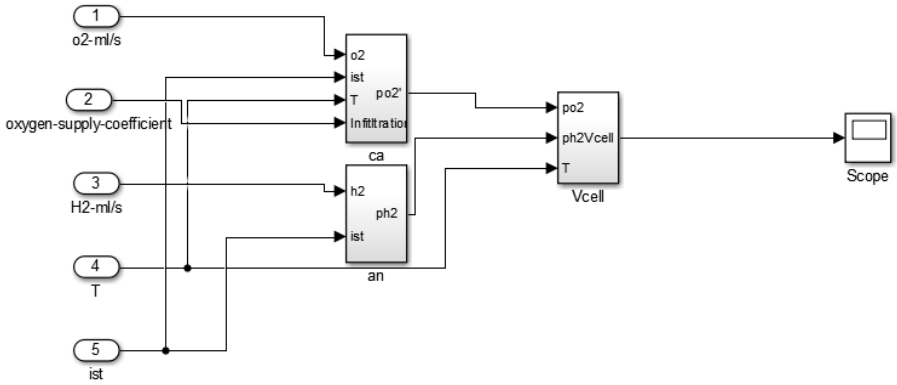

Figure 5. Schematic view of the model developed in the Simulink environment in order to simulate a fuel cell behavior under dynamic conditions.

The proposed actual-oxygen-supply-coefficient is employed to relax the gas diffusion, as not all the oxygen supplied to a single cell can be absorbed during actual operation. In Figure 6, the relevant voltage simulation data are shown. The data of MEAs with total thicknesses of 1.25 mm, 2.50 mm, and 3.75 mm are reported in the same figure in order to highlight how oxygen diffusion affects the performance of PEMFCs. By applying Equation (10), we can obtain values of the permeation capacity and the penetration time at different total thicknesses, which are listed in Table 2.

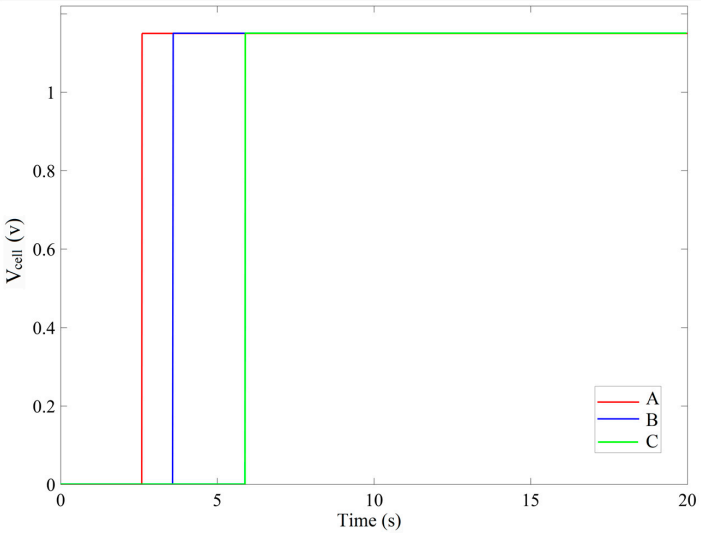

Figure 6. Comparison of simulation results (A) total thicknesses-1.25 mm (B) total thicknesses-2.50 mm (C) total thicknesses-3.75 mm.

Table 2. Permeation capacity of samples.

Simulation Results	Diffusion Layer Thickness (d)	Penetration Time (t_0)	Permeation Capacity (θ)
A	1.25 mm	3.0 s	6.1×10^{-5}
B	2.50 mm	3.6 s	5.1×10^{-5}
C	3.75 mm	5.9 s	3.1×10^{-5}

From the above figure, we can clearly see that the gas diffusion is a quick process. This time represents the influence of membranes, the performance of carbon paper, and environmental properties on gas diffusion. Some examples of influencing factors are the water content in the membrane, the temperature, the gas pressure, etc. This part of the process will not be discussed in this paper. After this period, the saturation voltage is obtained and the voltage remains a constant. Additionally, comparing the simulated and the real voltages, the proposed models slightly underestimate the actual performance of PEMFC, probably due to the simplifying assumptions. The permeation capacity can be calculated for certain diffusion layer materials based on the proposed model and the experimental results. The direct influence of permeation capacity is given for a single cell so that stack performance is significantly affected.

5. Conclusions

By developing a piecewise linearization model, a structural parameter is proposed to investigate the controllability of the cathode gas diffusion of PEMFCs. The key idea is to relax the relationship between the porosity of the cathode gas diffusion layer and carbon loading inside the cathode catalyst layer. The experiments and the simulations that are in a COMSOL and MATLAB/Simulink environment are introduced. The results show that the open circuit voltage strongly depends on the actual-oxygen-supply-coefficient. A large value of this parameter corresponds to a shorter penetration time and a quicker time for the voltage to reach a steady-state value. The steady-state value of the voltage is fixed along with the properties of the materials in the gas diffusion layer, which are strongly dependent on the actual-oxygen-supply-coefficient and the penetration time. Additionally, this duration decreases with an increase in the actual-oxygen-supply-coefficient. The electrodes with different gas diffusion layer total thicknesses have different coefficients, whose increases bring the decrease in coefficients. The cell could be controllably operated in a wide range of diffusion layer thicknesses by selecting the optimal value for the proposed parameter.

Author Contributions: Conceptualization, S.G.; methodology, S.G.; validation, X.Y. and S.G.; formal analysis, S.G.; writing—original draft preparation, S.G.; writing—review and editing, J.W. and X.Y.; supervision, Y.Z.; project administration, S.G. and Y.Z.; funding acquisition, S.G. and Y.Z. All authors have read and agreed to the published version of the manuscript.

Funding: This research was funded by the Natural Science Research of Jiangsu Higher Education Institutions of China 21KJD530002, the Industry University Research Cooperation Project in the Jiangsu Province of China BY2022786, and the Natural Science Foundation of Liaoning Province 2021BS062.

Data Availability Statement: Data and materials are available from the authors upon request.

Conflicts of Interest: The authors declare no conflict of interest.

Nomenclature

N	reacted moles of oxygen
I	individual cell current, A
t	time, s
α	actual-oxygen-supply-coefficient
γ	oxygen volumetric flow rate, mL/s
θ	permeation capacity
φ	flow influence factor
β	gas velocity, (m/s)
T	temperature of a single cell, K
S	effective surface area of the electrode, m^2
D	area of the gas tunnel cross-section, m^2
V_{cell}	a fuel cell voltage, V
E	electrode potential or thermodynamic potential, V
V_{act}	activation overvoltage, V

V_{ohmic}	ohmic overvoltage, V
E^0	standard electrode potential, V
t_0	penetration time, s
P_{H_2}	hydrogen partial pressure, bar
P_{O_2}	oxygen partial pressure, bar
d	thickness of diffusion layer, m

References

1. Tian, H.; Cui, X.; Shi, J. Emerging electrocatalysts for PEMFCs applications: Tungsten oxide as an example. *Chem. Eng. J.* **2021**, *421*, 129430. [CrossRef]
2. Chu, T.; Xie, M.; Yu, Y.; Wang, B.; Yang, D.; Li, B.; Ming, P.; Zhang, C. Experimental study of the influence of dynamic load cycle and operating parameters on the durability of PEMFC. *Energy* **2022**, *239*, 22356. [CrossRef]
3. Zhao, J.; Chang, H.; Luo, X.; Tu, Z.; Chan, S.H. A novel type of PEMFC-based CCHP system with independent control of refrigeration and dehumidification. *Appl. Therm. Eng.* **2022**, *204*, 117915. [CrossRef]
4. Jiao, D.; Jiao, K.; Zhong, S.; Du, Q. Investigations on heat and mass transfer in gas diffusion layers of PEMFC with a gas–liquid-solid coupled model. *Appl. Energy* **2022**, *316*, 118996. [CrossRef]
5. Deng, S.; Zhang, J.; Zhang, C.; Luo, M.; Ni, M.; Li, Y.; Zeng, T. Prediction and optimization of gas distribution quality for high-temperature PEMFC based on data-driven surrogate model. *Appl. Energy* **2022**, *327*, 120000. [CrossRef]
6. Herdem, M.S.; Farhad, S.; Hamdullahpur, F. Modeling and parametric study of a methanol reformate gas-fueled HT-PEMFC system for portable power generation applications. *Energy Convers. Manag.* **2015**, *101*, 19–29. [CrossRef]
7. Xu, Y.; Qiu, D.; Yi, P.; Lan, S.; Peng, L. An integrated model of the water transport in nonuniform compressed gas diffusion layers for PEMFC. *Int. J. Hydrog. Energy* **2019**, *44*, 13777–13785. [CrossRef]
8. Rahman, M.A.; Sarker, M.; Mojica, F.; Chuang, P.Y.A. A physics-based 1-D PEMFC model for simulating two-phase water transport in the electrode and gas diffusion media. *Appl. Energy* **2022**, *316*, 119101. [CrossRef]
9. Cindrella, L.; Kannan, A.M.; Lin, J.F.; Saminathan, K.; Ho, Y.; Lin, C.W.; Wertz, J. Gas diffusion layer for proton exchange membrane fuel cells-a review. *J. Power Sources* **2009**, *194*, 146–160. [CrossRef]
10. Xu, C.; Wang, H.; Cheng, T.A. Wave-shaped flow channel design and optimization of PEMFCs with a groove in the gas diffusion layer. *Int. J. Hydrog. Energy* **2023**, *48*, 4418–4429. [CrossRef]
11. He, P.; Mu, Y.T.; Park, J.W.; Tao, W.Q. Modeling of the effects of cathode catalyst layer design parameters on performance of polymer electrolyte membrane fuel cell. *Appl. Energy* **2020**, *277*, 115555. [CrossRef]
12. Wang, L.; Morales-Collazo, O.; Joan, F.B.; Jia, H. Dimeric ionic liquid for improving performance and durability of PEMFCs. *J. Power Sources* **2023**, *556*, 232488. [CrossRef]
13. Matamoros, L.; Brüggemann, D. Concentration and ohmic losses in free-breathing PEMFC. *J. Power Sources* **2007**, *173*, 367–374. [CrossRef]
14. Zhou, Z.; Ye, L.; Qiu, D.; Peng, L.; Lai, X. Experimental investigation and decoupling of voltage losses distribution in proton exchange membrane fuel cells with a large active area. *Chem. Eng. J.* **2023**, *452*, 139497. [CrossRef]
15. Pan, W.; Chen, Z.; Chen, X.; Wang, F.; Dai, G. Analytical and numerical investigation of flow distribution in PEMFC stacks. *Chem. Eng. J.* **2022**, *450*, 137598. [CrossRef]
16. Sun, Y.; Mao, L.; Wang, H.; Liu, Z.; Lu, S. Simulation study on magnetic field distribution of PEMFC. *Int. J. Hydrog. Energy* **2022**, *47*, 33439–33452. [CrossRef]
17. Ma, R.; Xie, R.; Xu, L.; Huang, Y.; Li, Y. A Hybrid Prognostic Method for PEMFC With Aging Parameter Prediction. *IEEE Trans. Transp. Electrif.* **2021**, *7*, 2318–2331. [CrossRef]
18. Zhao, Y.; Mao, Y.; Zhang, W.; Tang, Y.; Wang, P. Reviews on the effects of contaminations and research methodologies for PEMFC. *Int. J. Hydrog. Energy* **2022**, *45*, 23174–23200. [CrossRef]
19. Chugh, S.; Chaudhari, C.; Sonkar, K.; Sharma, A.; Kapur, G.S.; Ramakumar, S.S.V. Experimental and modelling studies of low temperature PEMFC performance. *Int. J. Hydrog. Energy* **2020**, *45*, 8866–8874. [CrossRef]
20. Kwon, O.J.; Shin, H.S.; Cheon, S.H.; Oh, B.S. A study of numerical analysis for PEMFC using a multiphysics program and statistical method. *Int. J. Hydrog. Energy* **2015**, *40*, 11577–11586. [CrossRef]
21. Behrou, R.; Pizzolato, A.; Forner-Cuenca, A. Topology optimization as a powerful tool to design advanced PEMFCs flow fields. *Int. J. Heat Mass Transf.* **2019**, *135*, 72–92. [CrossRef]
22. Nishimura, A.; Toyoda, K.; Kojima, Y.; Ito, S.; Hu, E. Numerical Simulation on Impacts of Thickness of Nafion Series Membranes and Relative Humidity on PEMFC Operated at 363 K and 373 K. *Energies* **2021**, *14*, 8256. [CrossRef]
23. Yu, X.; Zhang, C.; Fan, M.; Deng, B.; Huang, C.; Xu, J.; Liu, D.; Jiang, S. Experimental study of dynamic performance of defective cell within a PEMFC stack. *Int. J. Hydrog. Energy* **2022**, *47*, 8480–8491. [CrossRef]
24. Saeed, F.; Saidan, M.; Said, A.; Mustafa, M.; Abdelhadi, A.; Al-Weissi, S. Effect of flow rate, flow direction, and silica addition on the performance of membrane and the corrosion behavior of Pt–Ru/C catalyst in PEMFC. *Energy Convers. Manag.* **2013**, *75*, 36–43. [CrossRef]
25. Iulianelli, A.; Clarizia, G.; Gugliuzza, A.; Ebrasu, D.; Bevilacqua, A.; Trotta, F.; Basile, A. Sulfonation of PEEK-WC polymer via chloro-sulfonic acid for potential PEM fuel cell applications. *Int. J. Hydrog. Energy* **2010**, *35*, 12688–12695. [CrossRef]

26. Alberro, M.; Marzo, F.F.; Manso, A.P.; Domínguez, V.; Barranco, J.; Garikano, X. Electronic modeling of a PEMFC with logarithmic amplifiers. *Int. J. Hydrog. Energy* **2015**, *40*, 3708–3718. [CrossRef]
27. Pei, P.; Li, Y.; Xu, H.; Wu, Z. A review on water fault diagnosis of PEMFC associated with the pressure drop. *Appl. Energy* **2016**, *173*, 366–385. [CrossRef]
28. Yu, R.; Guo, H.; Ye, F.; Chen, H. Multi-parameter optimization of stepwise distribution of parameters of gas diffusion layer and catalyst layer for PEMFC peak power density. *Appl. Energy* **2022**, *324*, 119764. [CrossRef]
29. Meng, T.; Cui, D.; Ji, Y.; Cheng, M.; Tu, B.; Lan, Z. Optimization and efficiency analysis of methanol SOFC-PEMFC hybrid system. *Int. J. Hydrog. Energy* **2022**, *47*, 27690–27702. [CrossRef]
30. Musio, F.; Tacchi, F.; Omati, L.; Stampino, P.G.; Dotelli, G.; Limonta, S.; Brivio, D.; Grassini, P. PEMFC system simulation in MATLAB-Simulink®environment. *Int. J. Hydrog. Energy* **2011**, *36*, 8045–8052. [CrossRef]
31. Chesalkin, A.; Kacor, P.; Moldrik, P. Heat Transfer Optimization of NEXA Ballard Low-Temperature PEMFC. *Energies* **2021**, *14*, 2182. [CrossRef]